The Human-in-the-Loop Design Approach to the Longitudinal Automation System for an Intelligent Vehicle

Hsin-Han Chiang, *Member, IEEE*, Shinq-Jen Wu, Jau-Woei Perng, *Member, IEEE*, Bing-Fei Wu, *Senior Member, IEEE*, and Tsu-Tian Lee, *Fellow, IEEE*

***Abstract*—This paper presents a safe and comfortable longitudinal automation system which incorporates human-in-the-loop technology. The proposed system has a hierarchical structure that consists of an adaptive detection area, a supervisory control, and a regulation control. The adaptive detection area routes the information from on-board sensors to ensure the detection of vehicles ahead, particularly when driving on curves. Based on the recognized target distance from the adaptive detection area, the supervisory control determines the desired velocity for the vehicle to maintain safety and smooth operation in different modes. The regulation control utilizes a soft-computing technique and drives the throttle to execute the commanded velocity from the supervisory control. The feasible detection range is within 45 m, and the high velocity for the system operation is up to 100 km/h. The throttle automation under low velocity at 10–30 km/h can also be well managed by the regulation control. Numerous experimental tests in a real traffic environment exhibit the system's validity and achievement in the desired level of comfort through the evaluation of international standard ISO 2631-1.**

***Index Terms*—Adaptive cruise control (ACC), human-in-the-loop (HITL), intelligent vehicles, longitudinal vehicle control, transportation systems, vehicle automation.**

NOMENCLATURE

a_w	Frequency-weighted acceleration (in meters per second squared).
a_i	Root-mean-square (rms) acceleration for the Ith one-third octave band.
a	Distance from the center of gravity (CG) of vehicle to the front axle (in meters).
b	Distance from CG to the rear axle (in meters).
a_f	Acceleration of the following vehicle (in meters per second squared).
$a_{f\max}$	Constraint of maximum acceleration/deceleration (in meters per second squared).
a_p	Acceleration of the preceding vehicle (in meters per second squared).
C_f	Total cornering stiffness of the front tires (in newtons per radian).
C_r	Total cornering stiffness of the rear tires (in newtons per radian).
d	Distance from CG to the look-ahead point (in meters).
d_R	Distance in the feasible range of forward-looking sensor (in meters).
D_s	Signed distance in the fuzzy plane (error versus error change).
i_s	Steering ratio between the front-wheel angle and the steering wheel (SW) angle.
I_z	Yaw moment of inertia (in kilogram square meter).
k_t	Damping gain for conversion from the acceleration to the velocity.
L	Minimum distance or typical vehicle length (in meters).
m	Vehicle mass (in kilograms).
R_f	Radius of the curved road (in meters).
R	Measured distance between the preceding and the following vehicle (in meters).
R_{des}	Desired distance between the preceding and the following vehicle (in meters).
S	Sliding manifold.
S_h	Switching line in the fuzzy plane (error versus error change).
T	Period of the measurement (in seconds).
T_s	Sampling period in the control process (in seconds).
u_i	Consequent value of the ith rule output.
V_p	Forward velocity of the preceding vehicle (in meters per second).
V_f	Forward velocity of the following vehicle (in meters per second).
V_C	Commanded velocity for the following vehicle (in meters per second).
V_{des}	Driver-selected velocity for the following vehicle (in meters per second).
v_y	Lateral velocity in CG of the vehicle (in meters per second).

Manuscript received May 12, 2006; revised March 10, 2007. Date of publication March 11, 2010; date of current version June 16, 2010. This paper was recommended by Associate Editor C. M. Lewis.

H.-H. Chiang is with the Department of Electronic Engineering, Fu Jen Catholic University, Hsinchuang 24205, Taiwan (e-mail: hsinhan@ee.fju.edu.tw).

S.-J. Wu is with the Department of Electrical Engineering, Da-Yeh University, Changhua 51591, Taiwan (e-mail: jen@mail.dyu.edu.tw).

J.-W. Perng is with the Department of Mechanical and Electromechanical Engineering, National Sun Yat-Sen University, Kaohsiung 80424, Taiwan (e-mail: jwperng@faculty.nsysu.edu.tw).

B.-F. Wu is with the Department of Electrical and Control Engineering, National Chiao Tung University, Hsinchu 300, Taiwan (e-mail: bwu@cssp.cn.nctu.edu.tw).

T.-T. Lee is with the Department of Electrical and Control Engineering, National Chiao Tung University, Hsinchu 300, Taiwan, and also with the Department of Electrical Engineering, National Taipei University of Technology, Taipei 106, Taiwan (e-mail: ttlee@ntut.edu.tw).

Digital Object Identifier 10.1109/TSMCA.2010.2041925

r Yaw rate in CG of the vehicle (in radians per second).
W_i Weighting factor of interesting axes of body.
X_p Position of the preceding vehicle.
X_f Position of the following vehicle.
y_d Lateral offset from the centerline at a look-ahead distance (in meters).
ε_d Angle between the forward axis of the vehicle and the tangent to the road at a look-ahead distance (in radians).
δ_f Front-wheel angle of vehicle (in radians).
δ SW angle of vehicle (in radians).
θ Expanded angle in the adaptive detection area (in radians).
σ Desired headway time (in seconds).
λ Sliding surface gain.
α Slope of the switching line.
μ_i Membership function of the ith rule.

I. Introduction

VEHICLE automations are currently being introduced to relieve human drivers from the undesired routine tasks associated with driving. Since many studies have shown that most accidents are due to driver-related errors such as recognition and decision errors, the main initiative is considered for designing and developing safety systems that provide support to the driver to safely complete her/his driving tasks [1]–[3]. Therefore, vehicles with driver support systems have been developed as a way to reduce the number of car accidents and, at the same time, improve the traffic safety. With the rapid development of electronics and sensory technology, the potential benefits of vehicle automation are extensive. Moreover, such automation can be varied in both type and complexity. Indeed, it is possible to map out the entire process from conception to design and finally to execution [4].

Currently, the major emphasis has been placed on the field of driver's assistance rather than fully automated systems, and the transition from one type to the other can be implemented without costly modifications to vehicle manufacturers or to public infrastructure. Among these developments, longitudinal automation systems lead the more feasibility, and a number of theoretical and experimental researchers have already brought them into the realization in real vehicles [5]–[8]. The prior objective of these systems is to provide the speed-controlling assistance through throttle and brake driving. On this basis, cruise control (CC) and adaptive CC (ACC) systems have been developed for the market [5]. However, there are some existing limitations, such as the velocity constraint that the vehicle must drive at a speed greater than 40 km/h, and insufficient consideration of safety and comfort design requirements. The standard control design needs a mathematical model of the vehicle; however, it is not possible to obtain a complete model that comprises the complicated dynamics of a vehicle engine as well as the following motion with a forward vehicle. Moreover, the ill-conditioned and complex model of vehicle longitudinal dynamics encourages the employment of fuzzy logic control (FLC). In addition, FLC is capable of incorporating an expert's experience and representing human reasoning by using subjective and qualitative linguistic terms. It also anticipated that FLC could be an appropriate basis that accounts for human driving behaviors in a realistic manner [9], [19]. Nowadays, fuzzy controllers have been widely and effectively used in various vehicle control systems [9]–[12], [19].

Based on the fuzzy basis function network, a car-following collision prevention controller has been proposed [10]. Although the simulation results show the satisfactory performance of this controller, practical implementation is difficult due to the heavy computation required. In [11], the fuzzy control technique has been implemented on the velocity controller design of a golf car. Through experimental results involving the moving velocity of 2 m/s, their designed controller was found to be insensitive to parametric uncertainty and load fluctuations. The ACC controller based on fuzzy logic allied with a high-precision global positioning system, which is capable of assisting the driver in velocity and headway control, has been presented [12]. This proposed controller deals with the limitation of low velocity associated with conventional ACC systems; however, no transition between the CC and the ACC mode has been developed as information about the preceding vehicle's location and velocity are required to do that. Moreover, further essential requirements, such as safety strategies for car-following and curve capability, and driving comfort have not been evaluated yet. The potential success of the vehicle longitudinal automation system is to achieve safe driving control accompanied with ride comfort. Additionally, each type and level of automation should be primarily evaluated by examining its utilization associated with the consequences of human performance [4]. As a result, to increase the system's capability while involving the human driver, the conception of human-in-the-loop (HITL) needs to be more evident in the system's design.

The most important effect of incorporating HITL technology into automation system design is in the area of human safety, which also means that stability during the operation process of a system being achieved. The necessary safety consideration for vehicle longitudinal automation is the determination of the appropriate headway distance adjustment to avoid collision with the vehicle ahead. In the meantime, the system is able to follow a forward-moving vehicle even if that vehicle is cruising on curves with different radiuses [13]. To accommodate the automation system to meet the demands of different driving conditions, various operation modes that correspond to the transition frame need to be developed. With a human driver, there should be no initial demand for road environment, which can be viewed as a disturbance to the automation system. As we expect that a driver's behavior is complicated, particularly while complex tasks are being considered [14], it is essential to include adequate stability and robustness in the design of the controller. Following the guarantee of safety and stability of the longitudinal control system, ride quality performed by the system is the important consideration for automation design.

This paper proposes an HITL-based longitudinal automation system with more comprehensive functionalities than conventional ACC systems, as mentioned in previous references. The developed system with hierarchically configured structure comprises an adaptive detection area, a supervisory control, a

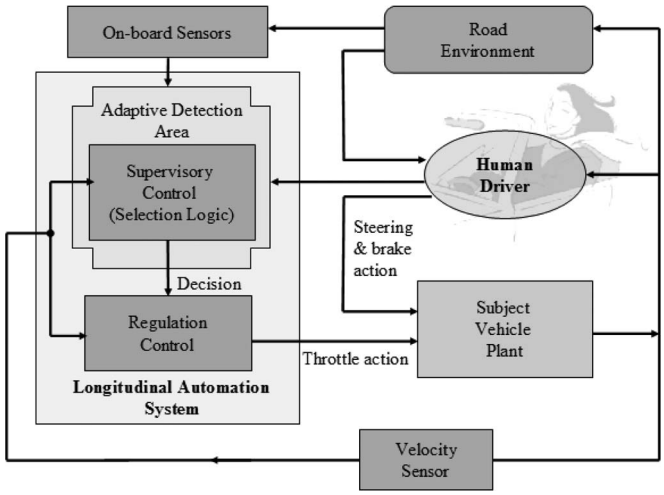

Fig. 1. Overall structure of the HITL longitudinal automation system.

regulation control, and special modifications to each segment of the automation system, which ensure safety and smooth operation. The main advantage to this type of structure is that once the lower level controller has been developed specifically for the vehicle, the upper level can be designed without much modification. Therefore, a reliable and robust higher level controller can be designed for the purpose of implementation on different vehicles with only minor tuning. With reference to the lower level controller, a human-like speed control that requires a soft-computing technique against the vehicle traction system's complexity and interdisturbance is required.

This paper is organized as follows. The proposed system configuration is introduced in Section II. Longitudinal automation system with the extension of HITL design is presented in Section III. Experimental results are included in Section IV, and the comfort evaluation is presented in Section V. Finally, the conclusion is given in Section VI.

II. System Configuration

The proposed longitudinal automation system with the interaction of a human driver and road environment is illustrated in Fig. 1. In this diagram, the road environment mainly refers to the longitudinal direction in front of the subject vehicle, and the on-board sensors include a forward-looking sensor (FLS), an SW angle sensor, and the speedometer of vehicle. This developed automation system has a hierarchical structure that is composed of an adaptive detection area, a supervisory control, and a regulation control. The adaptive detection area deals with the data from the on-board sensors according to the action of a human driver. Instead of horizontal detection in a fixed pattern, the adaptive detection area performs the adaptive action to guarantee that the preceding vehicle is detected on both straight and curved roads. Based on the recognized target distance, the supervisory control chooses the operation mode by using the defined control laws. The desired velocity command is conveyed to the regulation control for the execution of velocity tracking by producing the input signal of throttle degree to the throttle actuator. The brake pedal can be automated in the proposed mechanism, but it is not used in this study; namely,

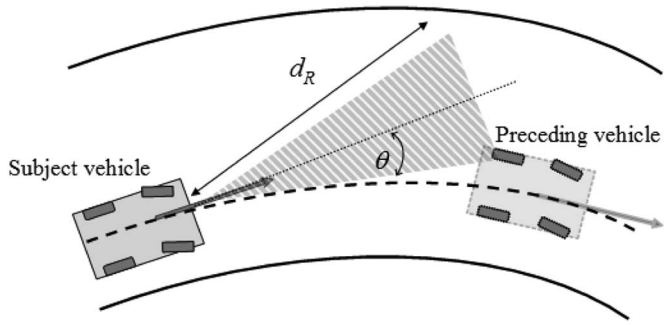

Fig. 2. Illustration of the scenario of vehicle following on curves.

the human driver needs to determine when should put on the brake pedal.

As far as the longitudinal automation incorporating a human driver is concerned, the controlling operations for the subject vehicle comprise the velocity cruise mode and vehicle following mode. In the former mode, the objective is to control the subject vehicle to track any desired velocity commanded by the human driver. When a forward vehicle is detected, the system will automatically switch to the latter mode which keeps a safe headway distance to the preceding vehicle. In addition, the system will automatically switch back to the velocity cruise mode if there is no vehicle detected ahead. Such a situation may arise when either vehicle changes lanes, or when the vehicle ahead increases its speed.

The safety of the vehicle following depends on the reliable detection of the distance between the preceding and the following vehicles. On straight roads, the headway distance can be measured from the FLS if it can be assumed that there is no failure in the sensor. However, failure to detect a vehicle ahead could arise due to curves in the road. In the specification of the international standard ISO 15622 [13], ACC systems are required to be provided with curve capability; i.e., the system should enable steady-state vehicles to follow with an appropriate headway distance on curves. As illustrated in Fig. 2, the preceding vehicle cannot be detected by the FLS of the following vehicle if the detection area is too narrow. Such a failure might result in instant acceleration. However, if the detection area is too broad, some unexpected objects near roadside might be detected which may cause the throttle to be off. The issue of curve capability, nonetheless, is still less considered in conventional longitudinal control systems. Therefore, it is necessary to design an adaptive detection maneuver so that the preceding vehicle can be correctly detected even when moving on curves.

In both these operation modes, the ride comfort of the human driver or passengers is considered as the evaluation of our longitudinal automation system. The international standard ISO 2631-1 [15], which defines the means to evaluate vibration levels with respect to human responses, is employed to examine the performed ride quality. This standard specifies direction and location of the measurements, the equipment to be used, duration of the measurements and frequency weighting, as well as the methods for the measurement and evaluation of the weight rms acceleration in meters per second squared. The index of this standard is determined by the frequency-weighted

TABLE I
CRITICAL THRESHOLD OF LIKELY REACTIONS IN ISO 2631-1 STANDARD

Vibration comfort	Frequency-weighted acceleration
Not uncomfortable	Less than 0.315 m/s^2
A little uncomfortable	0.315 to 0.63 m/s^2
Fairly uncomfortable	0.5 to 1 m/s^2
Uncomfortable	0.8 to 1.6 m/s^2
Very uncomfortable	1.25 to 2.5 m/s^2
Extremely uncomfortable	Greater than 2 m/s^2

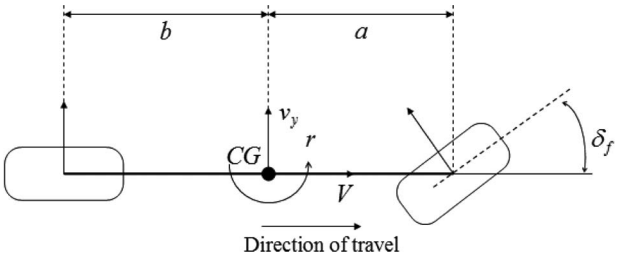

Fig. 3. Bicycle model diagram for vehicle lateral dynamics.

acceleration, which can be calculated by using the following expression:

$$a_w = \left[\sum_i (W_i\, a_i)^2\right]^{1/2}. \tag{1}$$

Comfort is assessed by ensuring that a_w over the sampled horizon does not reach a critical threshold value, as depicted in Table I. Notably, the evaluation of ride comfort for the longitudinal vehicle control mainly relies on the motion in the controlled vehicle's longitudinal axis. More details about the threshold value, the measurement points, and the frequency weighting are provided in [15].

There is no initial demand for road environment and the action of the human driver, which can be viewed as a disturbance to the automation system. The adequate stability and robustness is essentially factored into the control law appended with the designing criterion for ride comfort. The following section describes the designing methods.

III. LONGITUDINAL AUTOMATION SYSTEM DESIGN

In this section, the three components of the proposed vehicle longitudinal automation system are introduced.

A. Adaptive Detection Area

The turning behavior of a bicycle model depicted in Fig. 3 [6, Ch. 5] has been considered using the formula below in which the lateral dynamic from steering angle δ_f to lateral velocity v_y and yaw rate r is represented as

$$\begin{bmatrix} \dot{v}_y \\ \dot{r} \end{bmatrix} = A \begin{bmatrix} v_y \\ r \end{bmatrix} + B\delta_f \tag{2}$$

where

$$A = \begin{bmatrix} \frac{-(C_f+C_r)}{mV_f} & -V_f + \frac{-aC_f+bC_r}{mV_f} \\ \frac{-aC_f+bC_r}{I_zV_f} & \frac{-(a^2C_f+b^2C_r)}{I_zV_f} \end{bmatrix} \quad B = \begin{bmatrix} \frac{C_f}{m} \\ \frac{aC_f}{I_z} \end{bmatrix}.$$

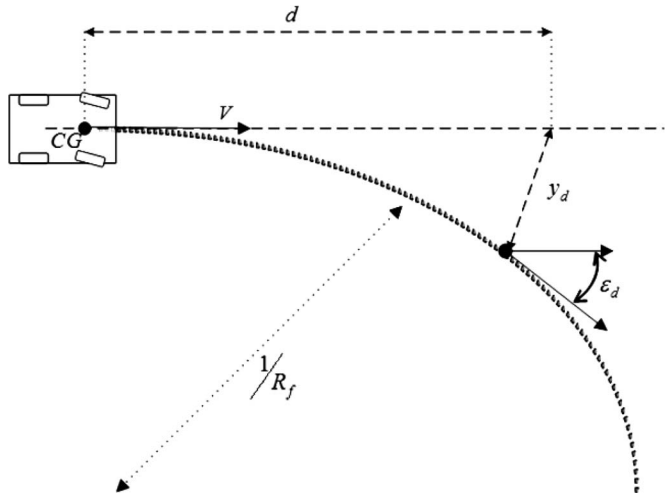

Fig. 4. Look-ahead evolution due to the vehicle motion and changes in the road geometry.

In addition to detecting the existence of the preceding vehicle, the look-ahead information of the subject vehicle (also referred to as the following vehicle) must be considered. Fig. 4 illustrates the vehicle traveling on a curve with a radius R_f. The equations capturing the evolution of the point at a look-ahead distance due to the motions of the vehicle and changes in the road geometry are the following:

$$\dot{y}_d = V_f\varepsilon_d - v_y - rd \tag{3}$$

$$\dot{\varepsilon}_d = V_f/R_f - r. \tag{4}$$

It should be noted that here the road curvature is constant due to the assumption of a steady-state analysis. The reason is that the vehicle will not reach a steady-state condition while traveling on a road with varying curvatures, and this makes it difficult to investigate the static relation. As shown in Fig. 2, the subject vehicle and the preceding vehicle both travel on a curve with a constant curvature of $1/R_f$. By considering a steady-state motion in which the subject vehicle tracks the curved road perfectly at a constant velocity, the variations of the vehicle lateral dynamics (2) and the look-ahead motion (3) and (4) can be set to zero, i.e., $\dot{v}_y = \dot{r} = \dot{y}_d = \dot{\varepsilon}_d = 0$. In the following, the subscript of ss denotes the value in the steady-state condition. By calculating the direction, the steady-state steering angle can be obtained as follows:

$$\delta_{\rm fss} = \frac{1}{R_f}\left(a + b - \frac{mV_f^2(aC_f - bC_r)}{(a+b)C_fC_r}\right). \tag{5}$$

The steady-state look-ahead lateral offset can be adopted as [17]

$$y_{\rm dss} = h_{\rm ss} - R_f \tag{6}$$

where $h_{\rm ss} = \sqrt{R_f^2 + d^2 + 2R_fd(-v_{\rm yss}/V_f)}$. Furthermore, at steady state, the lateral dynamics (2) can be represented as

$$A\begin{bmatrix} v_{\rm yss} \\ r_{\rm ss} \end{bmatrix} = -B\delta_{\rm fss} \tag{7}$$

and this holds if and only if

$$v_{\mathrm{yss}} = -r_{\mathrm{ss}} T \tag{8}$$

with $T = -b + amV_f^2/(a+b)C_r$. In (7), the term on the left-hand side is in the range space of matrix B. It should be noted that the fixed values of the yaw rate during the steady-state turning maneuver can be obtained by using

$$r_{\mathrm{ss}} = V_f / R_f. \tag{9}$$

By substituting (8) and (9) into (6), the steady-state look-ahead lateral offset can be rewritten as

$$y_{\mathrm{dss}} = \sqrt{R_f^2 + d^2 + 2dT} - R_f. \tag{10}$$

From (5) and (10), one obtains

$$\frac{y_{\mathrm{dss}}}{\delta_{\mathrm{fss}}} = \frac{R_f\sqrt{R_f^2 + d^2 + 2dT} - R_f^2}{\left(a + b - mV_f^2(aC_f - bC_r)/(a+b)C_fC_r\right)}. \tag{11}$$

It is also reasonable to assume that

$$|d^2 + 2dT|/R_f^2 \ll 1 \tag{12}$$

and the following approximation via Taylor's expansion can be obtained as

$$\sqrt{R_f^2 + d^2 + 2dT} = R_f + \frac{d^2 + 2dT}{2R_f}. \tag{13}$$

Through (13), (11) becomes

$$\frac{y_{\mathrm{dss}}}{\delta_{\mathrm{fss}}} = \frac{d^2 + 2dT}{2\left(a + b - V_f^2 P\right)} \tag{14}$$

where $P = m(aC_f - bC_r)/(a+b)C_fC_r$. It should be noted that P is also the understeer coefficient of the vehicle [16], [17]. By recalling Fig. 2, the following approximation can be applied:

$$y_{\mathrm{dss}} \simeq d_R \cdot \theta. \tag{15}$$

By substituting (14) into (15), one can obtain the relation from the steering angle to the adaptive detection angle as follows:

$$\frac{\theta}{\delta_{\mathrm{fss}}} = \frac{d^2 + 2dT}{2d_1\left(a + b - V_f^2 P\right)} =: \frac{K_\theta}{d_R}. \tag{16}$$

The steering angle can be substituted with the SW angle using a constant ratio $\delta = i_s \cdot \delta_f$ [18], [19]. Normally, the value of i_s is between 18 and 22 for passenger vehicles. In (16), the resulting feature is an adaptive ratio between the adaptive detection angle and the steering angle, which is independent of the road curvature. It can be observed that the adaptive ratio is updated as the vehicle velocity changes. The calculated y_{dss} refers to the offset between the point at the look-ahead distance and the position through which the vehicle will pass. When the vehicle is turning at a higher velocity, the look-ahead lateral offset increases such that the detection area expands in the same direction as the SW. Moreover, with respect to a reduced road curvature (or a longer radius), the look-ahead lateral offset decreases in that the detection area expands less. Table II depicts this result when $d = 42$ m and $d_R = 40$ m are given (as specified in the experiments).

TABLE II
(δ, θ) WITH VARYING VELOCITIES AND RADIUSES OF CURVES

V_f \ R_f	200m	300m	400m	500m
40 km/h	(19.6°, 6.9°)	(14.5°, 5.1°)	(10.9°, 3.8°)	(8.7°, 3.1°)
60 km/h	(23.9°, 9.2°)	(15.5°, 6.1°)	(11.6°, 4.6°)	(9.3°, 3.7°)
80 km/h	(25.1°, 11.9°)	(16.8°, 7.9°)	(12.6°, 5.9°)	(10.1°, 4.7°)
100 km/h	(27.6°, 16.6°)	(18.4°, 11.1°)	(13.8°, 8.3°)	(11.1°, 6.6°)

TABLE III
COMPARATIVE RESULTS BETWEEN ISO 15622 AND THE PROPOSED APPROACH

		ISO 15622	Adaptive detection area
Example 1 (R_f=500m)	y_{dss}	4.00 m	5.07 m
	θ	±3.70°	±4.61°
Example 2 (R_f=125m)	y_{dss}	4.60 m	4.83 m
	θ	±7.80°	±8.92°

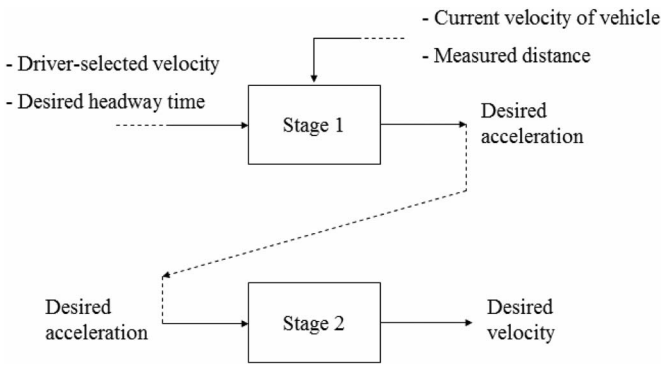

Fig. 5. Structure of the supervisory control.

Two calculations given in ISO 15622 are applied to verify the feasibility of the developed algorithm in (16). The two vehicles cruise on curve radiuses of 500 and 125 m with constant velocities of 31.67 and 16.94 m/s, respectively. The comparative results (the steady-state look-ahead lateral offset and the detection angle) between ISO 15622 and the proposed algorithm are presented in Table III. The evaluation criterion for the curves in ISO 15622 is dependent on the vehicle velocity and the lateral acceleration constraints. Furthermore, this criterion is a minimum requirement for the detection of the forward vehicle on the specified range of curves. The developed maneuver in (16) involves the major coefficients of the subject vehicle since they are derived from the lateral dynamics which determine the turning behavior of the vehicle. As a result, the proposed algorithm certainly satisfies the minimum requirement of ISO 15622 and provides a more confident detection range.

B. Supervisory Control Design

There are two stages in the supervisory control, as shown in Fig. 5. In the first stage, the desired acceleration of each

operation mode is determined. In the second stage, the desired acceleration is converted to the commended velocity. Unlike the conventional approaches (e.g., [6]–[8], [10], and [20]), which employ the calculated acceleration to control, the regulation control uses velocity-controlled loop since the vehicle's velocity can be directly measured for feedback. In this way, the problem of high-frequency noise that results from the sensed velocity differential is also prevented.

In the following, both the control strategies for the velocity cruise mode and the vehicle following mode are presented. For both control regimes, the sliding mode control (SMC) approach is adopted to design the corresponding control law. In the SMC, one proper surface S in the function of the system states is required, and the sliding manifold $S = 0$ defined on the closed-loop system is asymptotically stable. To achieve both reachable and sliding conditions, the following is required:

$$S\dot{S} < 0, \qquad S \neq 0 \tag{17}$$

where $\dot{S} = C(S)$ is a continuous function of S. The state trajectory can be forced to a stable manifold state $(S = 0)$ in a finite time interval according to its defined dynamics, and then, it slides toward equilibrium. With this type of SMC, the control law can be solved through the first derivative of the surface S.

The velocity cruise mode determines the desired acceleration at which the subject vehicle can track any velocity selected by the driver while avoiding any discomfort. The velocity tracking error can be defined as

$$e_V = V_f - V_{\rm des} \tag{18}$$

and the selected sliding surface as

$$S_{\rm VC} = e_V = V_f - V_{\rm des}. \tag{19}$$

In order for $S_{\rm VC}$ to approach zero, the following control law should be applied:

$$\dot{S}_{\rm VC} = -K_{\rm VC} S_{\rm VC} \tag{20}$$

where the constant parameter $K_{\rm VC} > 0$.

Equation (20) satisfies the global requirements of asymptotical stability and that $S_{\rm VC}\dot{S}_{\rm VC} < 0$. It should be noted that in typical literatures of SMC, the control law (20) usually includes a discontinuous sign function, e.g., $C(S_{\rm VC}) = -K_{\rm VC}S_{\rm VC} + k_0 {\rm sgn}(S_{\rm VC})$; this causes unexpected chattering accompanied with high-frequency noise. In this paper, a continuous function is chosen for implementation due to its simplicity.

By differentiating (19) and using (20), the desired acceleration will be obtained. To achieve the required ride comfort, the acceleration command should be maintained at the desired $a_{f\max}$, particularly while the initial value of e_V is large. Therefore, the sliding surface in (19) can be modified as

$$S_{\rm VC} = -a_f + a_{f\max} sat\left(\frac{a_f + e_V}{a_{f\max}}\right) \tag{21}$$

with

$$sat(x) = \begin{cases} x, & \text{as } |x| < 1 \\ sign(x), & \text{as } |x| \geq 1. \end{cases}$$

In the case of $|a_f + e_V| < a_{f\max}$, the sliding surface (21) is identical to that of (19), i.e., $S_{\rm VC} = e_V$. The desired acceleration can be solved as

$$a_{\rm VC} = \dot{V}_{\rm des} - K_{\rm VC} S_{\rm VC}. \tag{22}$$

When $|a_f + e_V| \geq a_{f\max}$, the sliding surface becomes

$$S_{\rm VC} = -a_f \pm a_{f\max} \tag{23}$$

and the desired acceleration is

$$a_{\rm VC} = \frac{-\dot{a}_f}{K_{\rm VC}} \pm a_{f\max}. \tag{24}$$

It should be noted that the jerk in (24) can be neglected in practice as it might prohibit the achievement of the desired acceleration $a_{\rm VC} = \pm a_{f\max}$.

The control laws in (22) and (24) are rather simple. Since only the velocity of the vehicle is required, implementation of this design and the requirement of ride comfort are both easy to achieve.

The objective of the vehicle following mode is to define a control law for the desired acceleration for headway distance tracking. In the development of a sliding surface, the vehicle following dynamics in terms of using the relative distance R are presented as

$$R = X_p - X_f \tag{25}$$

$$\dot{R} = V_p - V_f. \tag{26}$$

It has been demonstrated that string stability can be guaranteed if the design of the controller of the ACC is based on the fixed headway time strategy, i.e., the desired intervehicle distance is proportional to the vehicle velocity multiplying a constant time headway [20]. Moreover, the issue with regard to driver/passenger safety can then be taken into account (e.g., [5], [6], [13], [20], and [21]). By employing the fixed headway time strategy, the desired following distance law according to the velocity of the subject vehicle can be obtained by using

$$R_{\rm des} = \sigma V_f + L \tag{27}$$

$$\dot{R}_{\rm des} = \sigma a_f. \tag{28}$$

The error between the desired and relative headway distances is defined as

$$e_R = R - R_{\rm des}. \tag{29}$$

In the following, two designs with and without using vehicle-to-vehicle (v–v) communication are investigated.

With the consideration of bounded velocity variation, the sliding surface with the error and error variation can be defined as

$$S_{\rm VF} = -a_f + a_{f\max} sat\left(\frac{a_f + \dot{e}_R + \lambda e_R}{a_{f\max}}\right). \tag{30}$$

For the case of $|a_f + \dot{e}_R + \lambda e_R| < a_{f\max}$, the sliding surface becomes

$$\begin{aligned} S_{\rm VF} &= \dot{e}_R + \lambda e_R \\ &= \dot{R} - \dot{R}_{\rm des} + \lambda(R - R_{\rm des}). \end{aligned} \tag{31}$$

It is easy to examine the stability of the sliding surface in (31) by setting $S_{\rm VF} = 0$. The error dynamics $e_R(t) = e^{-\lambda t}$ is asymptotically stable for all positive λ. By differentiating (31), one obtains

$$\dot{S}_{\rm VF} = \ddot{R} - \ddot{R}_{\rm des} + \lambda(\dot{R} - \dot{R}_{\rm des}). \tag{32}$$

To guarantee the desired condition and asymptotic stability, the control law should be

$$\dot{S}_{\rm VF} = -K_{\rm VF} S_{\rm VF} \tag{33}$$

where the constant parameter $K_{\rm VF} > 0$.By virtue of (32) and (33), the desired acceleration can be achieved using the following equation:

$$a_{\rm VF} = \frac{1}{1 + \lambda\sigma}(K_{\rm VF} S_{\rm VF} + a_P + \lambda\dot{R} - \sigma\dot{a}_f). \tag{34}$$

While $|a_f + \dot{e}_R + \lambda e_R| \geq a_{f\max}$, the sliding surface becomes

$$S_{\rm VF} = -a_f \pm a_{f\max} \tag{35}$$

and the desired acceleration is

$$a_{\rm VF} = \frac{-\dot{a}_f}{K_{\rm VF}} \pm a_{f\max}. \tag{36}$$

It should be noted that the jerk of the following vehicle in (36) can be omitted in practice, i.e., $a_{\rm VF} = \pm a_{f\max}$.

Interestingly, while the acceleration of the following vehicle is primarily used in the sliding surface, it is erased in the final control form. Notably, the control law (34) needs the acceleration of the preceding vehicle a_p and the jerk of the following vehicle $\dot{a}_f$. These data are difficult to be directly measured in real time, and although the information of the preceding vehicle can be obtained by using a v–v communication system [3], it cannot be assumed that all vehicles have such a device. The jerk can be estimated using numerical methods, but it will increase computation cost. To overcome this disadvantage in (34), the sliding surface can be modified as

$$S_{\rm VF} = -a_f + a_{f\max} sat\left(\frac{a_f + e_R}{a_{f\max}}\right). \tag{37}$$

For the case of $|a_f + e_R| < a_{f\max}$, this sliding surface $S_{\rm VF} = e_R$ is stable as $e_R = 0$. By choosing the same control law as (33), the desired acceleration can be derived as

$$a_{\rm VF} = \frac{1}{\sigma}(K_{\rm VF} S_{\rm VF} + \dot{R}). \tag{38}$$

In addition, the result for the case of $|a_f + e_R| > a_{f\max}$ is the same as in (35) when the constraint $a_{\rm VF} = \pm a_{f\max}$ is employed. In (38), only the rate of headway distance is required. However, one can well imagine that a better performance will be achieved using the control law (34) since that additional knowledge can improve the controlling response of the following vehicle when compared to the behavior of the preceding one.

Remark: With conventional approaches to the consideration of ride quality, the calculated acceleration for the following vehicle is limited, i.e., if $|a_{\rm VF}| \geq a_{f\max}$, then $a_{\rm VF} = \pm a_{f\max}$. However, it cannot be guaranteed that the real acceleration of a vehicle will meet this criterion. Due to the fact that the actual acceleration is prevented from reaching the desired value by the saturation function of the sliding surface, our control law yields the condition of limiting the real acceleration of controlled vehicle. Finally, with respect to $a_{f\max}$, the value of 2.0 $\rm m/s^2$ is set in accordance with the specification of ISO 15622.

In the second stage, the conversion from the desired acceleration to the command velocity is achieved by using the following:

$$\dot{V}_C = a_{f\rm des} - k_t(V_f - V_C). \tag{39}$$

The suitable choice of k_t can avoid a sudden change of velocity due to sensor noise involved in the measurement of headway distance and vehicle velocity. To implement the conversion in appropriate time, the differential equation in (39) can be approximated by the following Euler's method:

$$V_C(k+1) = (1 - T_s k_t)V_C(k) + T_s(k_t V_f(k) + a_{f\rm des}(k)). \tag{40}$$

Then, the new value $V_C(k+1)$ can be computed given its past values $V_C(k)$, the current velocity $V_f(k)$, and the desired acceleration $a_{f\rm des}(k)$, as designed at the first stage. An autonomous scheme can select the desired mode by adopting the min-operation as

$$V_C(k+1) = \min\begin{cases} (1 - T_s k_t)V_C(k) + T_s(k_t V_f(k) + a_{\rm VC}(k)) \\ (1 - T_s k_t)V_C(k) + T_s(k_t V_f(k) + a_{\rm VF}(k)) \end{cases}. \tag{41}$$

The first half of (41) tends to track the command velocity for the subject vehicle operating in the velocity cruise mode. Once the preceding vehicle is detected, the system will automatically switch to the vehicle following mode, as shown in the second half of (41), which tends to keep a safe distance. This approach also conforms to the Gipps model, which has been demonstrated to be capable of longitudinal human driving characteristics [21].

C. Regulation Control Design

The objective of the regulation control is to execute the desired velocity command by the supervisory control. The vehicle longitudinal dynamics can be described using a system composed of various linear and nonlinear subsystems, e.g., engine, automatic transmission, brake, and the tires. Indeed, it is very difficult to design a control based on this complicated model. That is why we apply FLC to the problem of vehicle velocity regulation. In addition, a skilled driver's experiences can be incorporated into automatic throttle control via fuzzy logic reasoning. A fuzzy CC system with only four fuzzy rules achieving low velocity tracking performance is presented in [12].

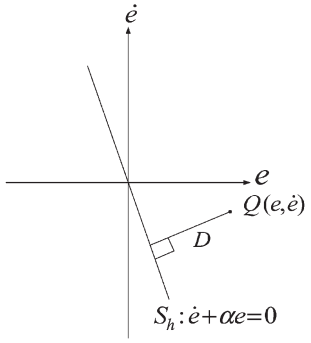

Fig. 6. Derivation of the signed distance.

For conventional FLCs, the fuzzy rule base has been constructed in 2-D space. The associated rule is described as follows:

$$R_{ij}:\ \text{If } e \text{ is } LE_i \text{ and } \dot{e} \text{ is } LDE_j,\ \text{then } u \text{ is } LU_{ij}$$

where LE, LDE, and LU are the linguistic term sets for the error e and the error change $\dot{e}$, where $i = 1, \ldots, M$ and $j = 1, \ldots, N$ indicate the number of term sets.It can be observed that many 2-D fuzzy rule bases have the so-called skew-symmetric property [22]. The switching line can be defined as

$$S_h:\ \dot{e} + \alpha e = 0. \tag{42}$$

The original fuzzy inputs of the error and error change can be combined into one signed distance, which is defined as the perpendicular distance, as illustrated in Fig. 6, from an operating point $Q(e, \dot{e})$ to the projection point on the switching line S_h as

$$\begin{aligned} D_s &= \text{sgn}(S_h) \cdot D \\ &= \text{sgn}(S_h) \cdot \frac{|\dot{e} + \alpha e|}{\sqrt{1+\alpha^2}} = \frac{\dot{e} + \alpha e}{\sqrt{1+\alpha^2}} \end{aligned} \tag{43}$$

with

$$\text{sgn}(S_h) = \begin{cases} 1, & \text{for } S_h > 0 \\ -1, & \text{for } S_h \le 0. \end{cases}$$

Now, the 2-D fuzzy rule base of the error and error change phase plane can be reduced into the 1-D space of D_s, and the associated rule can be reformulated as

$$R_i:\ \text{If } D_s \text{ is } LD_i,\ \text{then } u \text{ is } LU_i$$

where LD_i is the linguistic term for the signed distance in the ith rule.

Fig. 7 shows the closed-loop block diagram of the proposed regulation control. From (43), the equivalent proportional and derivative gains can then be obtained by

$$D_s = \frac{1}{\sqrt{1+\alpha^2}}\dot{e} + \frac{\alpha}{\sqrt{1+\alpha^2}}e = k_d\dot{e} + k_p e. \tag{44}$$

The regulation control scheme is composed of a proportional–derivative (PD) controller and an FLC. The input is $e = V_c - V_f$, and the output of the regulation control is u which presents the applied degree to the throttle actuator. The characteristics of the throttle actuator can be modeled as one saturation function with a transport delay $e^{-s\tau}$. The transfer function $H(s, V)$ presents the dynamics in terms of the transfer function from the applied throttle input to the vehicle velocity. The rule table is established on the 1-D space, as listed in Table IV: the fuzzy sets correspond to D_s are negative big (NB), negative small (NS), zero (ZO), positive small (PS), and positive big (PB), and the fuzzy sets correspond to u are negative big (NBu), negative small (NSu), zero (ZOu), positive small (PSu), and positive big (PBu). The membership functions for the fuzzy input D_s and the fuzzy output u are shown in Fig. 8, which depicts these two fuzzy partitions in the same normalized universe $[-1, 1]$.

The Center of Gravity (COG) method is applied to defuzzify the fuzzy outputs from the fuzzy inference machine to get the defuzzified output, i.e.,

$$u = \frac{\sum_{i=1}^{5} \mu_i(D_s) \times u_i}{\sum_{i=1}^{5} \mu_i(D_s)}. \tag{45}$$

There are many advantages for applying this PD-type SFLC: regardless of the controlled plant dynamics, it requires only one fuzzy input and a 1-D space of fuzzy rule base in contrast to both error and error change are required by conventional FLCs. If each of the five linguistic term sets is assigned to the error and the error change, a fuzzy rule table with 25 rules would result in arduous tuning. Therefore, the number of tuning parameters in the FLC can be significantly reduced from 25 to 5, and the computation load can also be considerably decreased while the control performance is nearly the same as that of conventional FLCs. The parameters k_p and k_d can be calculated beforehand instead of in an extra computation of the signed distance.

The vehicle longitudinal dynamics from the throttle voltage (or degree) to the vehicle velocity can be formed as a nonlinear function model of varying velocity [23]–[25]. Based on this model, the stability of the overall fuzzy control system under the effects of system parameters k_d and k_p and transport delay τ can be analyzed by the use of methods for the describing function approach, parameter space, and the Kharitonov approach. A systematic procedure to deal with this situation has been presented in our previous work [25]. Much information concerning limit cycles caused by the PD-type SFLC can be obtained using this approach, and the results show that the limit cycles can easily be suppressed if the system parameters are chosen carefully.

IV. Experimental Results

The testbed vehicle used in this study is a commercial vehicle, namely, Mitsubishi Savrian sedan 2.4 L, equipped with an automatic gearbox. A throttle-position sensor (TPS) associated with the throttle pedal was installed to measure the throttle degree. When the throttle pedal is depressed, the electrical signal from TPS is sent to the vehicle's engine control unit (ECU), and then, it adjusts the volume of the gasoline and air moving into the engine, which, in turn, causes the vehicle to move at a proportional velocity. For the sake of clarity, the structure of

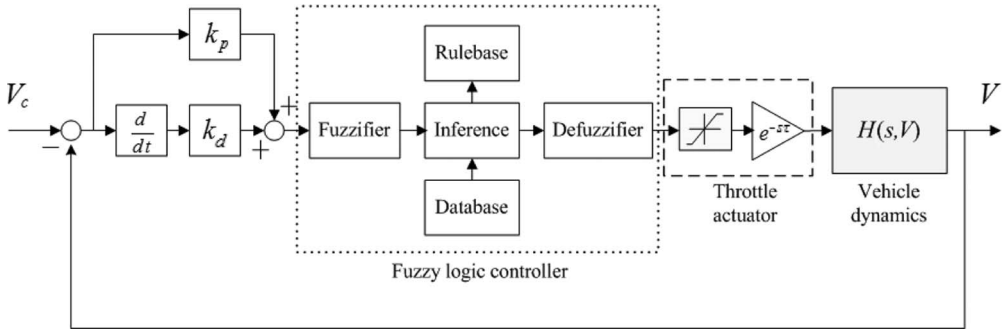

Fig. 7. Block diagram of the closed-loop velocity regulation control.

TABLE IV
FUZZY RULE BASE OF THE SFLC

D_s	NB	NS	ZO	PS	PB
u	NBu	NSu	ZOu	PSu	PBu

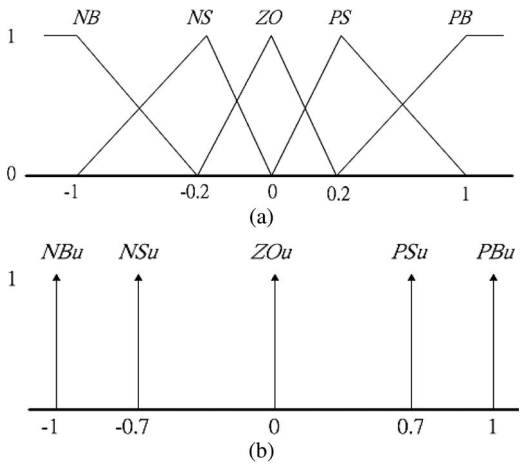

Fig. 8. (a) Membership functions of fuzzy input. (b) Membership functions of fuzzy output.

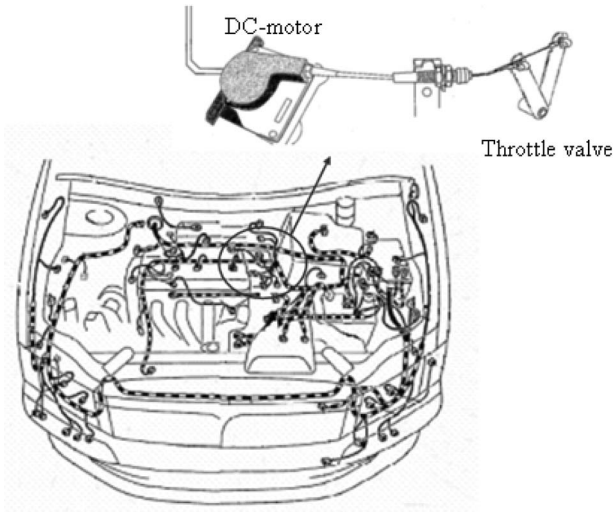

Fig. 9. Vehicle throttle body with the dc motor.

the proposed automation system is divided into the following parts:

1) *Core controller:* The designed longitudinal automation system is realized using a MicroAutoBox (MABX), a real-time digital-signal-processor-based hardware with a rapid prototype for control design and implementation, manufactured by the dSpace company. The MABX running the vehicle control software can be reprogrammed. The output of the MABX is the control throttle command to achieve velocity cruise and vehicle following.
2) *Utilized sensors:* The sensors utilized in the proposed system primarily measure the required dynamic states of the following vehicle. The velocity of the vehicle is measured by the speedometer and is transmitted to the MABX in the form of pulsewidth modulation signal. One accelerometer is used to measure the vehicle acceleration and deceleration in the direction of the longitudinal motion. The headway distance is measured by a laser range finder (LMS291, manufactured by SICK Company), and the data are sent to the interface board through the RS-232 bidirectional link. The permissible target detection range is specified to be within 82 m; however, in practice, the feasible detection distance is up to 45 m due to the high-speed motion of vehicles. The maximum angular coverage of the range finder is $\pm 50^\circ$ with a 1° minimum resolution in the azimuth plane. Initially, the width of detection area is set as $\pm 2^\circ$, which corresponds to driving on straight roads with zero SW angle. When the vehicle turns on a curve, the width of detection area is expended in accordance with the adaptive maneuver in (16).
3) *Throttle actuator:* The throttle valve has been adjusted using a mounted dc motor, as shown in Fig. 9. The purpose of this scheme is to prevent any change to the vehicle's internal components. If the throttle pedal is depressed tighter by the driver rather than the dc motor, then the car will respond to the driver. The throttle degree sensor used in this study is a frequent analog-to-digital converter that encodes the analog voltage output from the TPS into a digital value in the normalized interval. This digital signal is used as a feedback signal and sent to the MABX for throttle control.

To reinforce the credibility of the proposed system, the controlled vehicle has been tested on real traffic environments. To establish the validity of the proposed system, many experiments have been conducted on an expressway, where the highest legal velocity is 90 km/h. Fig. 10 shows a snapshot of the car-following experiment. Initially, there are two experimental vehicle platforms used for testing, but only the following vehicle activates the longitudinal automation system. The preceding

Fig. 10. Snapshot of the car-following experiment on expressway.

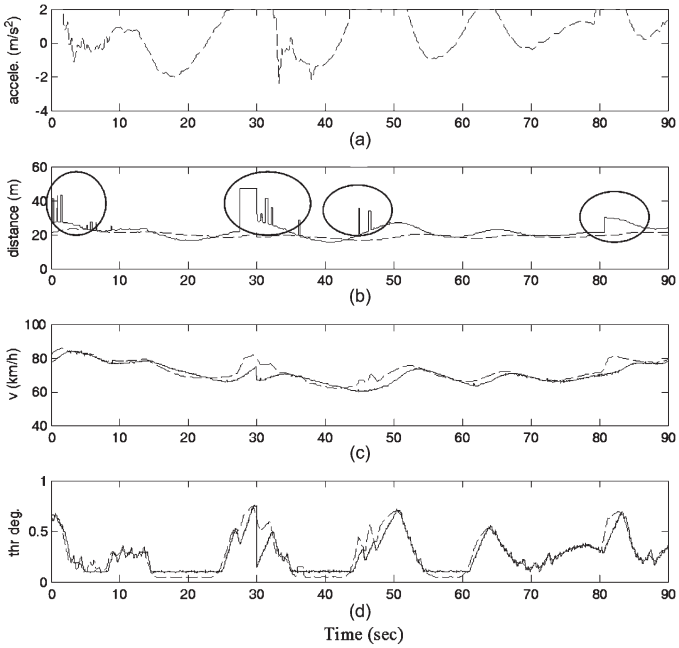

Fig. 11. Sampled history of vehicle following experiments without adaptive detection area maneuver (dashed line: reference signal; solid line: real signal).

vehicle is driven manually to simulate the unpredictable driving maneuvers of the vehicle ahead.

The sample history of the car-following experiments without the employment of the adaptive detection area is depicted in Fig. 11. Here, the headway time σ is set as 1 s, which is the minimum requirement of ISO 15622. Fig. 11(d) shows the applied throttle degree, which ranged from 0.13 (pedal fully released) to 0.82 (pedal fully pressed). Fig. 11(c) displays the desired velocity (dashed line) and current velocity (solid line) of the controlled vehicle. The desired headway distance (broken line) and the measured distance (solid line) from the range finder are shown in Fig. 11(b). The desired acceleration (with the bounded $a_{f\max}$ of 2 m/s^2) calculated from the supervisory control is depicted in Fig. 11(a).

As evident in Fig. 11(b), some apparent pulse signals (illustrated in the circled area) exist at the signal of the intervehicle distance measured from the range finder. This is because at this instant, the preceding vehicle is undetected by the range finder due to the fact that the forward vehicle moving outside

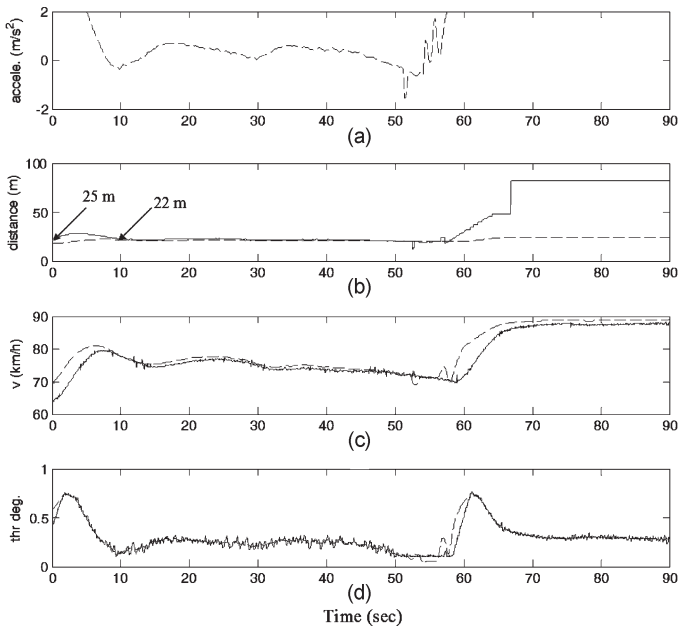

Fig. 12. Sampled history of experiments involving the transition between the vehicle following mode and velocity cruise mode (dashed line: reference signal; solid line: real signal).

of detected area (target missing). This situation occurs when the two vehicles move on curves with an approximate radius of 400 m, particularly when the following vehicle is driven near the outside edge while the preceding vehicle is driven near the inside edge of the road. In Fig. 11(a), it can be seen that the calculated acceleration fluctuates dramatically. In this situation, the system switches to the higher velocity CC mode, which causes the command of the throttle voltage to become erratic, as shown in Fig. 11(d). Consequently, for a vehicle velocity of 80–60–80 km/h, the initial detection angle of $\pm 2^\circ$ is deficient when compared to the required detection angle in the adaptive detection maneuver ($\pm 4.6^\circ$–5.9°; refer to Table II). Although the human driver can apply the brake to avoid the sudden acceleration of the controlled vehicle, such an action may not be desired due to the simultaneous actuation of throttle and brake.

Fig. 12 depicts the sample history of experiments that involved the employment of the adaptive detection area. In contrast to Fig. 11(b), there was no pulse signal in Fig. 12(b). This indicates that no target-missing detection occurred while the vehicles moved over the same curves with a radius of approximately 400 m. Initially, the subject vehicle moved with a velocity of 65 km/h, and one vehicle ahead is detected at 25 m, but it is outside of the desired operation range (18 m for the headway time $\sigma = 1$ s). Once the subject vehicle accelerates to nearly 80 km/h and the preceding vehicle is within the operation range of 22 m at time $= 10$ s, as shown in Fig. 12(b), the system adjusts the throttle to keep the desired headway distance for the vehicle following mode. During the vehicle following process (from 10 to 50 s), not only does the subject vehicle track the desired velocity successfully, as shown in Fig. 12(c), but it also maintains the desired headway distance [in Fig. 12(b)] with respect to the preceding vehicle despite the velocity variation within [70, 80] km/h.

When the preceding vehicle changes to the neighboring lane at 60 s, as shown in Fig. 12, the system identifies the condition

in which there is no vehicle ahead. Thus, the subject vehicle automatically switches to the velocity cruise mode and accelerates to the preset velocity of 88 km/h. As illustrated in Fig. 12(c), after the 60 s point, the velocity of the subject vehicle converges smoothly to the reference velocity profile. If one vehicle moves into the lane in the forward direction, or a vehicle with a slower velocity is detected ahead within the feasible range, then the throttle pedal will be adjusted to follow the preceding vehicle while maintaining a safe distance. Likewise, the operation at low velocity (10 km/h upward) can also be handled by the proposed regulation control against the system nonlinearity including gear changes and a torque converter of a vehicle engine. This fact shows the advantage of employing FLC due to its robust characteristics and capacity to cope with disturbances.

V. Comfort Evaluation

The primary gauge to determine vibration and ride comfort is the vehicle's acceleration along the interesting of direction. As a result, during these experimental tests on the longitudinal automation system, the level of comfort for driver/passenger can be evaluated by means of the measured acceleration history on the longitudinal axis. In the experiment, an accelerometer is located at the CG of the vehicle to measure the longitudinal acceleration history. As specified in ISO 2631-1, the vibration evaluation procedures incorporate methods to average vibration over time and frequency bands. The running flow of evaluation procedures, which is in accordance with ISO 2631-1, is summarized as follows.

1) Obtain the acceleration data from an accelerometer.
2) Compute the rms acceleration of the ith one-third octave band in accordance with the following equation or its equivalents in the frequency domain:

$$a_w = \left[\frac{1}{T}\int_0^T a_w^2(t)dt\right]^{\frac{1}{2}}. \tag{46}$$

Remark: The equivalents of the rms acceleration in the frequency domain can be calculated by applying *Parseval's Theorem* [26, Ch. 2], i.e.,

$$\sum_n |x[n]|^2 = \frac{1}{2\pi}\int_{-\pi}^{\pi} \left|X(e^{j\omega})\right|^2 d\omega. \tag{47}$$

The function $X(e^{j\omega})$ denotes the energy density spectrum since it determines the energy distribution in the frequency domain.

3) Determine the frequency-weighted acceleration in accordance with (1) in which the weighting factor (as specified in ISO 2631-1 [15]) for the x-direction is utilized.

The experiments for the performed vehicle's velocities and accelerations at low speed (10–30 km/h), normal speed (40–60 km/h), and high speed (60–90 km/h) controlling operations are displayed in Fig. 13 in which the broken line indicates the desired velocity and the solid line represents the measured velocity of the vehicle. The evaluation results are summarized in Table V. The operations at low speed and normal speed

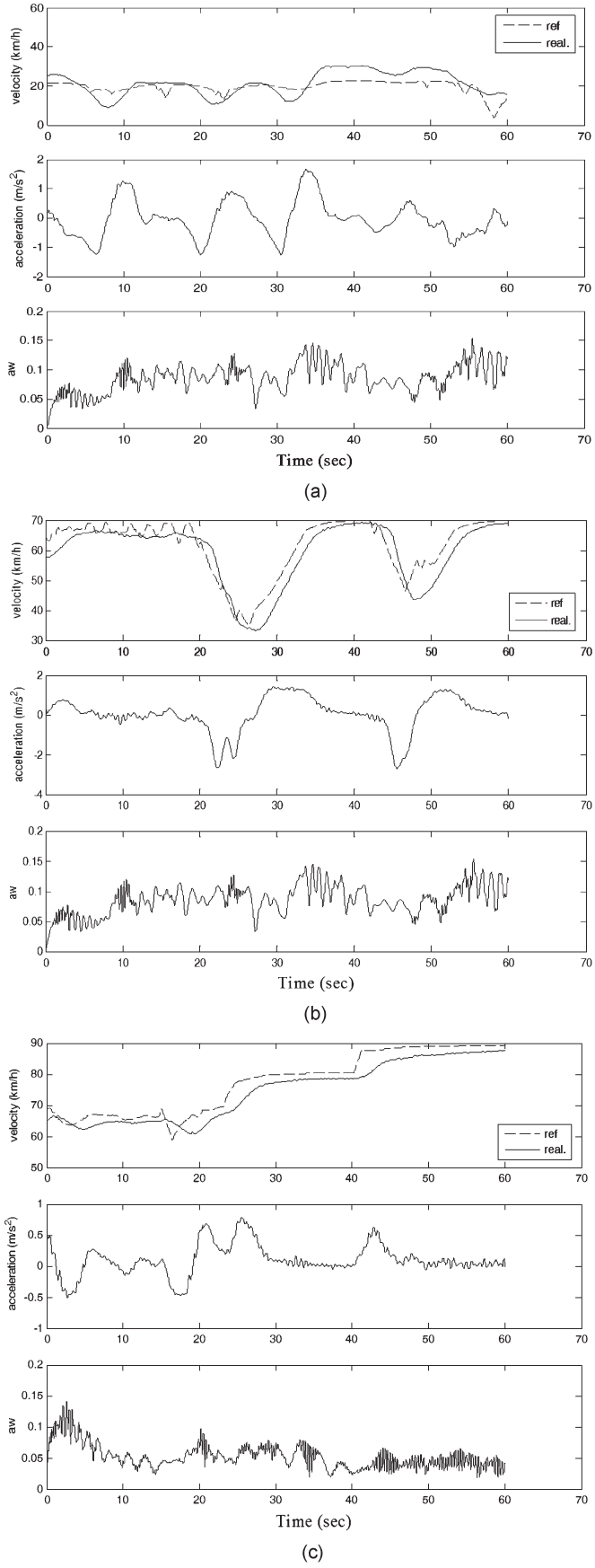

Fig. 13. (a) Ride quality evaluation under low-speed operation (10–30 km/h). (b) Ride quality evaluation under normal-speed operation (40–60 km/h). (c) Ride quality evaluation under high-speed operation (60–90 km/h).

TABLE V
RIDE QUALITY EVALUATION RESULTS UNDER DIFFERENT OPERATION SPEEDS

Indices / Velocity range	Max. acceleration	Max. a_w	Averaged a_w	ISO 2631-1 deg.
10—30 km/h	1.72 m/s^2	0.151	0.092	Not uncomfortable
40—60 km/h	1.79 m/s^2	0.152	0.108	Not uncomfortable
60—90 km/h	0.78 m/s^2	0.101	0.051	Not uncomfortable

were undertaken in the urban-like environment, and those at high speed were conducted on an expressway/highway. The measured accelerations of the vehicle in each operation are all less than the constraint of 2 m/s^2, which is required by the proposed design. As can be observed in Table V, the primary index for ride quality a_w in each operation velocity range is far less than 0.315, and this result implies that the ride quality is "Not uncomfortable," as specified by ISO 2631-1.

VI. CONCLUSION

Integration of HITL design into a longitudinal automation design has been presented in this paper, and the overall system was implemented on a passenger vehicle and successfully verified in real traffic environments. The proposed system has a comprehensive structure, which is composed of the adaptive detection area, the supervisory control, and the regulation control, in terms of a hierarchical form that can be implemented on different vehicles with only minor tuning. The system's safety has been improved by the inclusion of the proposed adaptive detection maneuver to prevent the target missing of a preceding vehicle on curves. The supervisory control determines the control mode without the need for v–v communication and operates stably within the constrained acceleration profile. As to the execution of throttle control, the regulation control has been designed based on an understanding of the operation of human reasoning and with the objective of reducing the number of rules required. The proposed automation system is designed to assist the human driver with regard to the velocity and intervehicle space control to reduce the driving burden, particularly in a long trip. Finally, the experimental results in real traffic environments demonstrate not only the validity of the longitudinal automation system, but also the ride comfort achieved based on an evaluation using standard ISO 2631-1.

REFERENCES

[1] P. Varaiya, "Smart cars on smart roads: Problems of control," *IEEE Trans. Autom. Control*, vol. 38, no. 2, pp. 195–207, Feb. 1993.

[2] K. Yamada and J. K. Kuchar, "Preliminary study of behavioral and safety effects of driver dependence on a warning system in a driving simulator," *IEEE Trans. Syst., Man, Cybern. A, Syst., Humans*, vol. 36, no. 3, pp. 602–609, May 2006.

[3] I. Chisalita and N. Shahmehri, "On the design of safety communication systems for vehicles," *IEEE Trans. Syst., Man, Cybern. A, Syst., Humans*, vol. 37, no. 6, pp. 933–945, Nov. 2007.

[4] R. Parasuraman, T. B. Sheridan, and C. D. Wickens, "A model for types and levels of human interaction with automation," *IEEE Trans. Syst., Man, Cybern. A, Syst., Humans*, vol. 30, no. 3, pp. 286–297, May 2000.

[5] A. Vahidi and A. Eskandarian, "Research advances in intelligent collision avoidance and adaptive cruise control," *IEEE Trans. Intell. Transp. Syst.*, vol. 4, no. 3, pp. 143–153, Sep. 2003.

[6] H. Raza and P. Ioannou, "Vehicle following control design for automated highway systems," *IEEE Trans. Control Syst. Technol.*, vol. 16, no. 6, pp. 43–60, Dec. 1996.

[7] R. Rajamani, S. B. Choi, B. K. Law, J. K. Hedrick, R. Prohaska, and P. Kretz, "Design and experimental implementation of longitudinal control for a platoon of automated vehicles," *Trans. ASME, J. Dyn. Syst. Meas. Control*, vol. 122, no. 3, pp. 470–476, Sep. 2000.

[8] K. Yi and Y. D. Kwon, "Vehicle-to-vehicle distance and speed control using an electronic-vacuum booster," *JSAE Rev.*, vol. 22, no. 4, pp. 403–412, Oct. 2001.

[9] X. Qu and M. A. Nussbaum, "Simulating human lifting motions using fuzzy logic control," *IEEE Trans. Syst., Man, Cybern. A, Syst., Humans*, vol. 39, no. 1, pp. 109–118, Jan. 2009.

[10] J. Mar, F. J. Lin, H. T. Lin, and L. C. Hsu, "The car following collision prevention controller based on the fuzzy basis function network," *Fuzzy Sets Syst.*, vol. 139, no. 1, pp. 167–183, Oct. 2003.

[11] K. R. S. Kodagoda, W. S. Wijesoma, and E. K. Teoh, "Fuzzy speed and steering control of an AGV," *IEEE Trans. Control Syst. Technol.*, vol. 10, no. 1, pp. 112–120, Jan. 2002.

[12] J. E. Naranjo, C. Gonzalez, J. Reviejo, R. Garcia, and T. de Pedro, "Adaptive fuzzy control for inter-vehicle gap keeping," *IEEE Trans. Intell. Transp. Syst.*, vol. 4, no. 3, pp. 132–142, Sep. 2003.

[13] Transportation Information and Control Systems—Adaptive Cruise Control Systems—Performance Requirements and Test Procedures, ISO 15622, 2002.

[14] J. H. Kim, S. Hayakawa, T. Suzuki, K. Hayashi, S. Okuma, N. Tsuchida, M. Shimizu, and S. Kido, "Modeling of driver's collision avoidance maneuver based on controller switching model," *IEEE Trans. Syst., Man, Cybern. B, Cybern.*, vol. 35, no. 6, pp. 1131–1143, Dec. 2005.

[15] Mechanical Vibration and Shock-Evaluation of Human Exposure to Whole-body Vibration—Part 1: General Requirements, ISO 2631/1, 1997.

[16] J. Y. Wong, *Theory of Ground Vehicles*. New York: Wiley, 2001.

[17] K. A. Unyelioglu, E. Hatipoglu, and U. Ozguner, "Design and stability analysis of a lane following controller," *IEEE Trans. Control Syst. Technol.*, vol. 5, no. 1, pp. 127–134, Jan. 1996.

[18] S. J. Wu, H. H. Chiang, J. W. Perng, T. T. Lee, and C. J. Chen, "The automated lane-keeping design for an intelligent vehicle," in *Proc. Intell. Veh. Symp.*, Las Vegas, NV, 2005, pp. 508–513.

[19] S. J. Wu, H. H. Chiang, J. W. Perng, C. J. Chen, B. F. Wu, and T. T. Lee, "The heterogeneous systems integration design and implementation for lane keeping on a vehicle," *IEEE Trans. Intell. Transp. Syst.*, vol. 9, no. 2, pp. 246–263, Jun. 2008.

[20] P. A. Ioannou and C. C. Chien, "Autonomous intelligent cruise control," *IEEE Trans. Veh. Technol.*, vol. 42, no. 4, pp. 657–672, Nov. 1993.

[21] Z. Bareket, P. S. Fancher, H. Peng, K. Lee, and C. A. Assaf, "Methodology for accessing cruise control behavior," *IEEE Trans. Intell. Transp. Syst.*, vol. 4, no. 3, pp. 123–131, Sep. 2003.

[22] B. J. Choi, S. W. Kwak, and B. K. Kim, "Design stability analysis of single-input fuzzy logic controller," *IEEE Trans. Syst., Man, Cybern. B, Cybern.*, vol. 30, no. 2, pp. 303–309, Apr. 2000.

[23] G. M. Takasaki and R. E. Fenton, "On the identification of vehicle longitudinal dynamics," *IEEE Trans. Autom. Control*, vol. AC-22, no. 4, pp. 610–615, Aug. 1977.

[24] A. S. Hauksdüttir and G. Sigurardóttir, "On the use of robust design methods in vehicle longitudinal controller design," *Trans. ASME, J. Dyn. Syst. Meas. Control*, vol. 115, no. 3, pp. 166–172, Mar. 1993.

[25] J. W. Perng, B. F. Wu, H. I. Chin, and T. T. Lee, "Limit cycle analysis of uncertain fuzzy vehicle control systems," in *Proc. IEEE Int. Conf. Netw., Sens., Control*, Tucson, AZ, 2005, pp. 626–631.

[26] A. V. Oppenheim, R. W. Schafer, and J. R. Buck, *Discrete-Time Signal Processing,* 2nd ed. Englewood Cliffs, NJ: Prentice-Hall, 1999.

[27] E. Pennestri, P. P. Valentini, and L. Vita, "Comfort analysis of car occupants: Comparison between multibody and finite element models," *Int. J. Veh. Syst. Model. Test.*, vol. 1, no. 1/2, pp. 68–78, Jan. 2005.

Hsin-Han Chiang (S'02–M'04) received the B.S. and Ph.D. degrees in electrical and control engineering from the National Chiao-Tung University, Hsinchu, Taiwan, in 2001 and 2007, respectively.

He was a Postdoctoral Researcher in electrical engineering from the National Taipei University of Technology, Taipei, Taiwan, in 2008 and 2009, respectively. He is currently an Assistant Professor with the Department of Electronic Engineering, Fu Jen Catholic University, Hsinchuang, Taiwan. His research interests include intelligent systems design, fuzzy systems and control, automated vehicle control, and intelligent transportation systems.

Shinq-Jen Wu received the B.S. degree in chemical engineering from the National Taiwan University, Taipei, Taiwan, in 1986, the M.S. degree in chemical engineering from the National Tsing-Hua University, Hsinchu, Taiwan, in 1989, the M.S. degree in electrical engineering from the University of California, Los Angeles, in 1994, and the Ph.D. degree in electrical and control engineering from the National Chiao-Tung University, Hsinchu, in 2000.

From September 1989 to July 1990, she was with the Laboratory for Simulation and Control Technology, Chemical Engineering Division, Industrial Technology Research Institute, Hsinchu. In 1991, she joined the Department of Chemical Engineering, Kao-Yuan Junior College of Technology and Commerce, Kaohsiung, Taiwan. From 1995 to 1996, she was an Engineer with the Integration Engineering Department, Macronix International Company Ltd., Hsinchu. She is currently with the Department of Electrical Engineering, Da-Yeh University, Changhwa, Taiwan. She is the Editor of *Advances in Fuzzy Sets and Systems* (Pushpa Publishing House, India). Her research interests include ergonomics-based smart cars, advanced vehicle control and safety systems, Petri-net modeling for cancer mechanisms, robust identification of genetic networks, soft sensor for on-line tuning, soft-computation-based protein structure prediction, VLSI process technology, optimal fuzzy control/tracking, optimal fuzzy estimation, and soft-computation modeling techniques.

Dr. Wu is a member of Phi Tau Phi. Her name is included in the *2006 Asian Admirable Achievers*, 2007 *Asian/Pacific Who's Who*, and 2008–2009 *Marquis Who's Who in Science and Engineering* (10th anniversary edition).

Jau-Woei Perng (S'02–M'04) was born in Hsinchu, Taiwan, in 1973. He received the B.S. and M.S. degrees in electrical engineering from the Yuan Ze University, Chungli, Taiwan, in 1995 and 1997, respectively, and the Ph.D. degree in electrical and control engineering from the National Chiao Tung University (NCTU), Hsinchu, Taiwan, in 2003.

From 2004 to 2008, he was a Research Assistant Professor with the Department of Electrical and Control Engineering, NCTU. He is currently an Assistant Professor with the Department of Mechanical and Electromechanical Engineering, National Sun Yat-Sen University, Kaohsiung, Taiwan. His research interests include robust control, nonlinear control, fuzzy logic control, neural networks, systems engineering, and intelligent vehicle control.

Bing-Fei Wu (S'89–M'92–SM'02) was born in Taipei, Taiwan, in 1959. He received the B.S. and M.S. degrees in control engineering from National Chiao Tung University (NCTU), Hsinchu, Taiwan, in 1981 and 1983, respectively, and the Ph.D. degree in electrical engineering from the University of Southern California, Los Angeles, in 1992.

Since 1992, he has been with the Department of Electrical Engineering and Control Engineering, NCTU, where he is currently a Professor. He has been involved in the research of intelligent transportation systems for many years and leads a research team to develop the first Taiwan smart car, TAIWAN *i*TS-1, with autonomous driving and active safety system. His current research interests include vision-based vehicle driving safety, intelligent vehicle control, multimedia signal analysis, embedded systems, and chip design.

Prof. Wu is the Founder and was the Chair of the IEEE Systems, Man, and Cybernetics Society Taipei Chapter in 2003. From 1999 to 2000, he was the Director of the Control Technology of Consumer Electronics Research Group, Automatic Control Section, National Science Council, Taiwan. As an active Industry Consultant, he was involved in the chip design and applications of the Flash memory controller and 3C consumer electronics in multimedia systems, for which he received the Best Industry–Academics Cooperation Research Award from the Ministry of Education in 2003. He received the Xerox–Fujitsu Academic Research Award in 2007, the Distinguished Engineering Professor Award from the Chinese Institute of Engineers in 2002, the Outstanding Information Technology Elite Award from the Taiwan Government in 2003, the First Prize Award of TI China–Taiwan DSP Design Contest in 2006, the Outstanding Research Award in 2004 from NCTU, the Golden Acer Dragon Thesis Award sponsored by the Acer Foundation in 1998 and 2003, respectively, the First Prize Award of the We Win (Win by Entrepreneurship and Work with Innovation and Networking) Competition hosted by the Industrial Bank of Taiwan in 2003, and the Silver Award of Technology Innovation Competition sponsored by the Advantech Foundation in 2003.

Tsu-Tian Lee (M'87–SM'89–F'97) received the B.S. degree in control engineering from the National Chiao-Tung University (NCTU), Hsinchu, Taiwan, in 1970 and the M.S. and Ph.D. degrees in electrical engineering from the University of Oklahoma, Norman, in 1972 and 1975, respectively.

In 1975, he was an Associate Professor with the Department of Control Engineering, NCTU, where he became a Professor and the Chairman in 1978. In 1981, he became a Professor and the Director of the Institute of Control Engineering, NCTU. In 1986, he was a Visiting Professor with the University of Kentucky, Lexington, where he became a Full Professor of electrical engineering in 1987. In 1990, he was a Professor and the Chairman of the Department of Electrical Engineering, National Taiwan University of Science and Technology, Taipei, Taiwan, where he became a Professor and the Dean of the Office of Research and Development in 1998. Since 2000, he has been with the Department of Electrical and Control Engineering, NCTU, where he is currently a Chair Professor. He has also been with the Department of Electrical Engineering, National Taipei University of Technology, since 2004, where he is currently the President.

Prof. Lee received the Distinguished Research Award from the National Science Council in 1991–1998, the Academic Achievement Award in Engineering and Applied Science from the Ministry of Education in 1997, the National Endow Chair from the Ministry of Education in 2003, and the TECO Science and Technology Award from the TECO Technology Foundation in 2003. He was elected to the grade of IEE Fellow in 2000. He became a Fellow of the New York Academy of Sciences in 2002. He has served as a Member of the Technical Program Committee and a Member of Advisory Committee for many IEEE-sponsored international conferences. He is currently the Vice President of Membership, a member of the Board of Governors, and the Newsletter Editor for the IEEE Systems, Man, and Cybernetics Society.